

# A Computational Pipeline for Patient-Specific Modeling of Thoracic Aortic Aneurysm: From Medical Image to Finite Element Analysis

Jiasong Chen<sup>a</sup>, Linchen Qian<sup>a</sup>, Ruonan Gong<sup>a</sup>, Christina Sun<sup>b</sup>, Tongran Qin<sup>b</sup>, Thuy Pham<sup>b</sup>, Caitlin Martin<sup>b</sup>, Mohammad Zafar<sup>c</sup>, John Elefteriades<sup>c</sup>, Wei Sun<sup>b</sup>, Liang Liang<sup>\*a</sup>

<sup>a</sup> Department of Computer Science, University of Miami, Coral Gable, FL, USA

<sup>b</sup> Sutra Medical Inc, Lake Forest, CA, USA

<sup>c</sup> Aortic Institute at Yale-New Haven Hospital, Yale University School of Medicine, New Haven, CT, USA

## 1. DESCRIPTION OF PURPOSE

The aorta is the body's largest arterial vessel, serving as the primary pathway for oxygenated blood within the systemic circulation<sup>1</sup>. Aortic aneurysms consistently rank among the top twenty causes of mortality in the United States<sup>2</sup>. Thoracic aortic aneurysm (TAA) arises from abnormal dilation of the thoracic aorta and remains a clinically significant disease, ranking as one of the leading causes of death in adults<sup>3</sup>. A thoracic aortic aneurysm ruptures when the integrity of all aortic wall layers is compromised due to elevated blood pressure. Currently, three-dimensional computed tomography (3D CT) is considered the gold standard for diagnosing TAA. The geometric characteristics of the aorta, which can be quantified from medical imaging, and stresses on the aortic wall, which can be obtained by finite element analysis (FEA), are critical in evaluating the risk of rupture and dissection.

Deep learning-based image segmentation has emerged as a reliable method for extracting anatomical regions of interest from medical images<sup>4-6</sup>. Voxel-based segmentation masks of anatomical structures are typically converted into structured mesh representation to enable accurate simulation. Hexahedral meshes are commonly used in finite element simulations of the aorta due to their computational efficiency and superior simulation accuracy<sup>7</sup>. Due to anatomical variability, patient-specific modeling enables detailed assessment of individual anatomical and biomechanics behaviors, supporting precise simulations, accurate diagnoses, and personalized treatment strategies. Finite element (FE) simulations provide valuable insights into the biomechanical behaviors of tissues and organs in clinical studies. Developing accurate FE models represents a crucial initial step in establishing a patient-specific, biomechanically based framework for predicting the risk of TAA<sup>8</sup>. For example, Sun et al. observed distinct mechanical patterns in the aorta associated with dissection and subsequent repair through patient-specific finite element stress analysis<sup>9</sup>.

The aim of this research is to develop a complete computational workflow for patient-specific thoracic aortic aneurysm modeling, covering all key steps from segmentation to mesh generation and finite element simulation.

## 2. METHODS

The proposed computational pipeline/workflow is illustrated in Figure 1, which consists of three main stages: segmentation, meshing, and simulation. The segmentation stage extracts the aorta geometry from 3D CT images, represented by a mesh with an arbitrary number of nodes and elements and a random topology. The meshing stage converts the segmented aorta geometry (i.e., a random mesh) into a quadrilateral surface mesh with a pre-defined topology, which is then converted to a solid hexahedral mesh with appropriate wall thickness. Finally, using the solid mesh, the simulation stage performs patient-specific FE simulations to obtain wall stress distributions. This pipeline connects raw CT images to the final patient-specific aortic wall stress assessment.

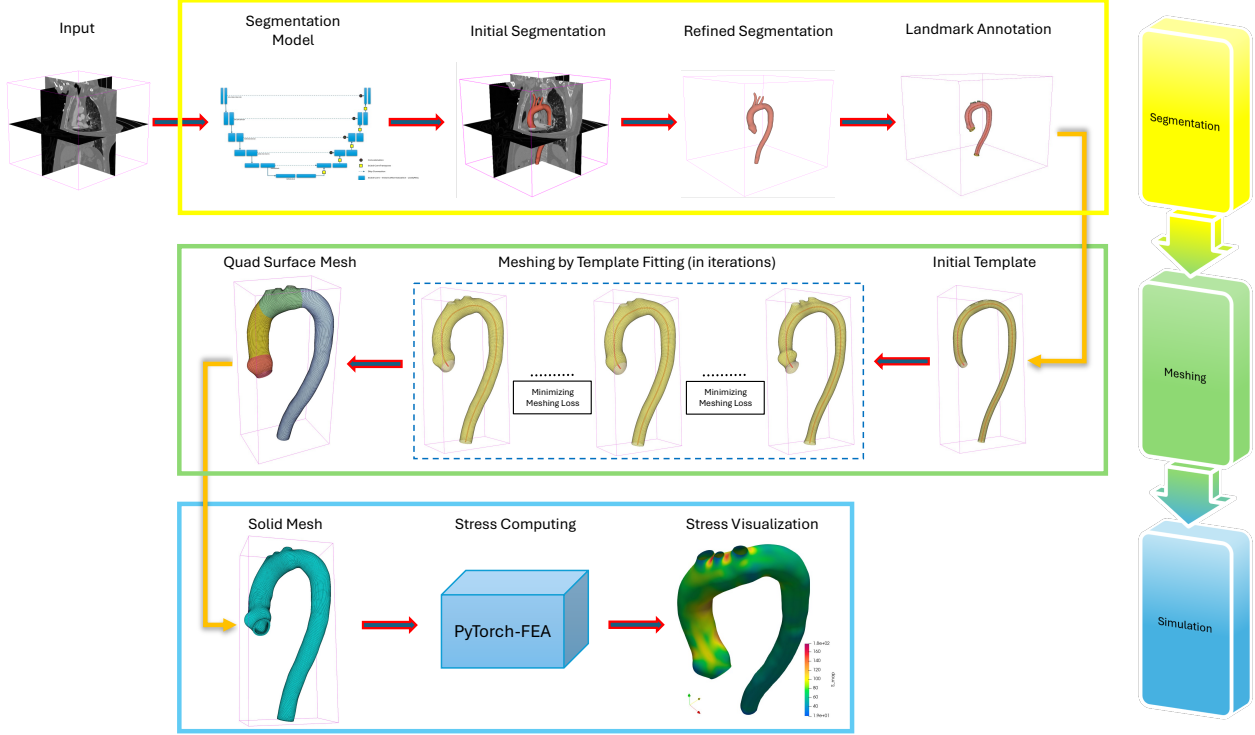


Figure 1. Pipeline Diagram

## 2.1 Dataset

Two public datasets and one in-house dataset were utilized, with all data fully de-identified. The first public dataset, the HOCM dataset<sup>10</sup>, includes 27 CT scans from patients with a history of septal myectomy surgery. The second public dataset, INSPECT<sup>11</sup>, is a multimodal medical dataset containing data from 19,402 patients for pulmonary embolism diagnosis and prognosis. The in-house dataset, obtained from Yale University – New Haven Hospital, includes 47 patients, comprises both individuals without TAA and those with TAA or Type A aortic dissections, with images acquired at multiple time points.

## 2.2 Segmentation

The segmentation stage consists of three steps: initial segmentation using a deep learning-based segmentation model, segmentation refinement, and annotation of anatomical landmarks.

Various deep learning-based segmentation models can be employed, including nnU-Net<sup>12</sup>, TransUNet<sup>13</sup>, Swin UNETR<sup>14</sup>, MedSAM<sup>15</sup>. In this study, the nnU-Net framework was selected to perform the segmentation task. nnU-Net utilizes a straightforward U-Net architecture combined with a highly optimized pipeline, achieving state-of-the-art segmentation performance. The network consists of an encoder path for down-sampling and a decoder path for up-sampling, forming a U-shaped configuration with skip connections between the encoder and decoder. Different U-Net variants can be integrated within the nnU-Net architecture. We trained the nnU-Net model using 47 patients from the Yale dataset and 27 patients from the HOCM dataset. The training objective was to minimize a combination of Dice loss and standard cross-entropy loss between the ground truth and predicted segmentation masks, as defined in Eq. (1) and Eq. (2). Further details regarding the segmentation models are provided in our previous work<sup>16</sup>.

$$\mathcal{L} = \mathcal{L}_{Dice} + \mathcal{L}_{CE} \quad (1)$$

$$\mathcal{L}_{Dice} = 1 - \frac{2 \sum_{i,j} (y(i,j) \hat{p}_m(i,j))}{\sum_{i,j} (y(i,j) + \hat{p}_m(i,j))} \quad (2)$$

Following initial segmentation, manual refinement was performed to correct possible errors from the nn-Unet output, in order to ensure accurate aorta geometry. Three experts independently reviewed and iteratively refined the segmentations until a consensus was reached.

Once the segmentation results are finalized, anatomical landmarks—including hinge points, aortic arch curves, end curves, centerline, and maximal inner sphere radius—are manually annotated by three experts using the 3D slicer software<sup>17</sup>. The annotation process is repeated until consensus is reached. The three hinge points define the hinge curve, serving as the inlet of the aorta geometry. The end curve defines the outlet of the aorta geometry, located at the celiac trunk artery branch on a plane perpendicular to the descending aorta. Aortic arch curves are positioned approximately 2 mm above the contact points between the branch vessels and the aortic main body. The aortic centerline consists of 320 points, and the corresponding maximal inner sphere radius are used in the subsequent meshing stage to generate the initial quadrilateral mesh template.

### 2.3 Meshing

In the meshing stage, the process begins with the generation of an initial quadrilateral mesh template, which is subsequently deformed to match the aorta geometry obtained from the segmentation stage. This stage is fully automatic and implemented using the PyTorch library.

The initial quadrilateral mesh template is constructed as a tubular mesh. This tube is generated using 320 cross-sections perpendicular to the centerline, each centered on a point along the aorta centerline and with a radius equal to the corresponding maximal inner sphere radius. The centerline's start point is defined as the center of the three hinge points, and the end point corresponds to the end curve center. Each cross section (i.e., a circumference curve) consists of 78 evenly spaced points. The first cross-section lies on the hinge points plane and last cross-section lies on the end curve plane. To generate cross-sections ( $G$ ), each centerline point ( $C$ ) and its associated radius ( $r$ ) establish a local coordinate system defined by the tangent vector ( $T$ ), normal vector ( $N$ ), and binormal vector ( $B$ ). At each centerline point, each of the cross-section points ( $P_i$ ) are generated according to Eq. (3). Subsequently, a quadrilateral mesh is constructed by connecting points between adjacent cross-sections. The arrangement of quad corners for vertices ( $i$ ) in cross-sections  $G_j$  and  $G_{j+1}$  follows Eq. (4). Finally, the initial mesh template is completed by cutting holes in the aortic arch region of the mesh, corresponding to the patient-specific number of aortic arch branches.

$$P_i(\theta) = r_i \cos \theta N_i + r_i \cos \theta B_i + C_i, \theta \in \{0, 2\pi\} \quad (3)$$

$$\text{Quad Corner } (G_j, G_{j+1}) = (P_{i,j}, P_{i+1,j}, P_{i+1,j+1}, P_{i,j+1}) \quad (4)$$

In Eq. (4),  $P_{i,j}$  denotes the point  $i$  on the cross-section  $j$ . After generating the initial quadrilateral mesh template, a template fitting module deforms it to match the patient-specific aorta geometry obtained from the segmentation stage, using a designed meshing loss in Eq. (5) which measures the difference between the ground-truth mesh  $S_{gt}$  and template mesh  $S_{template}$ , combining Chamfer loss with a mesh quality loss. The mesh quality loss includes element surface loss, surface flatness loss, element angle loss, and other element-quality related terms. Through iterative optimization, the template mesh deforms into a patient-specific quadrilateral aortic mesh, and the chamfer distance error between  $S_{gt}$  and  $S_{template}$  becomes sufficiently small.

$$\text{meshing Loss} = \text{chamfer\_loss}(S_{gt}, S_{template}) + \text{mesh\_quality\_loss}(S_{gt}, S_{template}) \quad (5)$$

### 2.4 Simulation

The PyTorch-FEA library<sup>18</sup> was used for finite element (FE) simulation in this study to obtain the stress distribution on the aortic wall under the normal systolic blood pressure of 16kPa. 100 patients without aneurysms were selected from the INSPECT dataset, serving as the control group, and 37 patients with TAA were selected from the in-house dataset (Yale dataset). We implemented the Static Determinacy Approach (SDA) in the PyTorch-FEA library for FE simulations, which does not need patient-specific material properties. The details of SDA were reported in our previous work<sup>9</sup>, where commercial software Abaqus was used. Because the FE meshes have node and element correspondence among patients, FE simulations are fully automatic with our open-source software PyTorch-FEA.

### 3. RESULTS

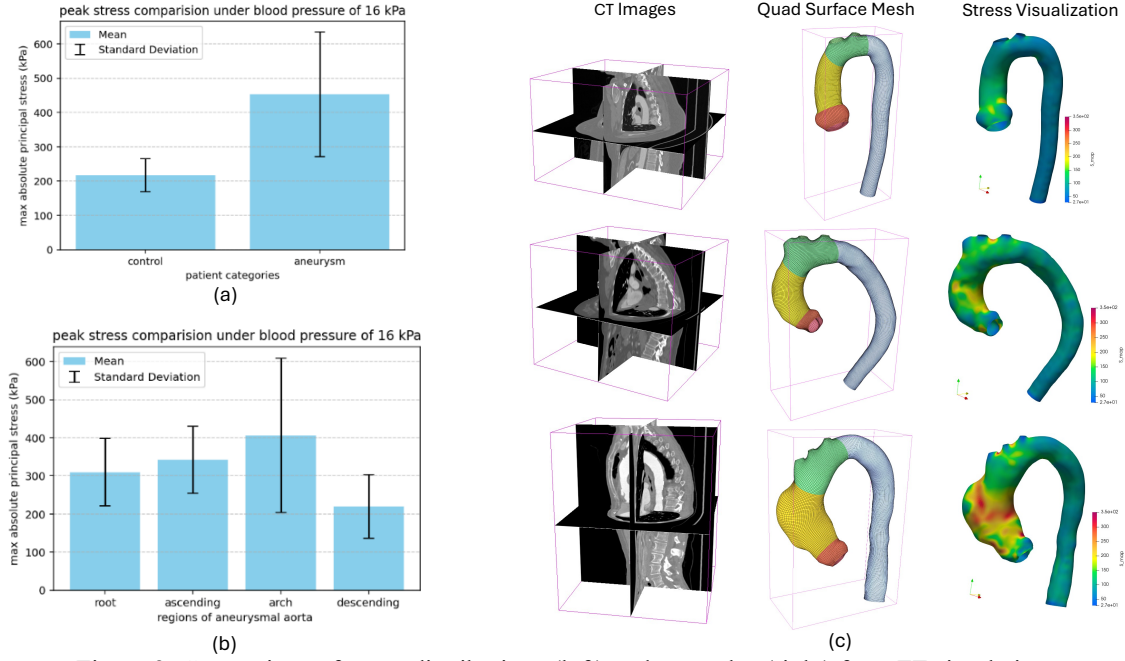


Figure 2. Comparison of stress distributions (left) and examples (right) from FE simulations.

We compared stress analysis results between the non-aneurysm patients (control group) and the 37 aneurysm patients from the Yale dataset (aneurysm group). As shown in Figure 2a, aneurysm patients exhibited both higher maximum absolute principal wall stress and greater standard deviation. These findings demonstrate that our pipeline can capture clinically relevant biomechanical differences that may aid in thoracic aortic aneurysm diagnosis.

We analyzed stress distribution across different aortic regions, including the aortic root, ascending aorta, aortic arch, and descending aorta. In the aneurysmal patients (Figure 2b), the distribution of maximum absolute principal stress showed the highest values in the aortic arch, followed by the ascending aorta, aortic root, and descending aorta. These findings suggest that our pipeline can reveal region-specific biomechanical insights, providing more detailed disease assessment and supporting personalized treatment planning. The findings are consistent with our previous works<sup>9</sup>, which relied on a fully manual workflow.

Figure 2c shows pipeline outputs at the meshing and simulation stages for one non-aneurysm patient and two aneurysmal patients. The FE simulations show substantially increased wall stress concentrated within the dilated portions of the aorta in severe aneurysm cases, which implies stresses are risk indicator of TAA.

### 4. NEW OR BREAKTHROUGH WORK TO BE PRESENTED

- (1) We developed a comprehensive computational pipeline for patient-specific modeling of thoracic aortic aneurysms, combining segmentation, mesh generation, and finite element simulation. A key innovation of this pipeline is the open-arch mesh with node and element correspondence among different patients, enabled by the template-fitting based meshing method, which preserves anatomical accuracy, enables statistical shape modeling<sup>19</sup>, and facilitates FE simulations with all-hexahedral elements in PyTorch-FEA—capabilities not addressed in previous studies.
- (2) Our pipeline captures clinically relevant biomechanical differences, showing that aneurysm patients exhibit significantly higher maximum absolute principal stress, which may aid in thoracic aortic aneurysm diagnosis. Our pipeline quantifies stress distribution across different regions of the aorta, enabling more detailed disease assessment and supporting personalized treatment planning.
- (3) We will open-source the pipeline on GitHub.

### 5. CONCLUSION

We present a comprehensive computational pipeline for patient-specific thoracic aortic aneurysm modeling, integrating segmentation, meshing, and finite element simulation. The framework highlighted clinically relevant biomechanical patterns, including elevated wall stress in aneurysmal patients and region-specific stress distributions. These findings emphasize the potential of our pipeline to enhance patient-specific disease assessment and support personalized treatment planning for thoracic aortic aneurysm.

**ACKNOWLEDGEMENT:** This work was supported in part by the NIH grant R01HL158829

## REFERENCES

- [1] Shahoud, J. S., Miao, J. H. and Bolla, S. R., “Anatomy, Thorax, Heart Aorta,” [StatPearls], StatPearls Publishing, Treasure Island (FL) (2025).
- [2] “WISQARS Leading Causes of Death Visualization Tool.”, Centers for Disease Control and Prevention, <<https://wiscqars.cdc.gov/lcd/>> (18 August 2025 ).
- [3] Kuzmik, G. A., Sang, A. X. and Elefteriades, J. A., “Natural history of thoracic aortic aneurysms,” *Journal of Vascular Surgery* **56**(2), 565–571 (2012).
- [4] Wang, R., Lei, T., Cui, R., Zhang, B., Meng, H. and Nandi, A. K., “Medical image segmentation using deep learning: A survey,” *IET Image Processing* **16**(5), 1243–1267 (2022).
- [5] Conze, P.-H., Andrade-Miranda, G., Singh, V. K., Jaouen, V. and Visvikis, D., “Current and Emerging Trends in Medical Image Segmentation With Deep Learning,” *IEEE Transactions on Radiation and Plasma Medical Sciences* **7**(6), 545–569 (2023).
- [6] Chen, C., Qin, C., Qiu, H., Tarroni, G., Duan, J., Bai, W. and Rueckert, D., “Deep Learning for Cardiac Image Segmentation: A Review,” *Front. Cardiovasc. Med.* **7** (2020).
- [7] Liang, X., Ebeida, M. S. and Zhang, Y., “Guaranteed-quality all-quadrilateral mesh generation with feature preservation,” *Computer Methods in Applied Mechanics and Engineering* **199**(29–32), 2072–2083 (2010).
- [8] Wisneski, A. D., Mookhoek, A., Chitsaz, S., Hope, M. D., Guccione, J. M., Ge, L. and Tseng, E. E., “Patient-Specific Finite Element Analysis of Ascending Thoracic Aortic Aneurysm,” *J Heart Valve Dis* **23**(6), 765–772 (2014).
- [9] Sun, C., Qin, T., Kalyanasundaram, A., Elefteriades, J., Sun, W. and Liang, L., “Biomechanical stress analysis of Type-A aortic dissection at pre-dissection, post-dissection, and post-repair states,” *Computers in Biology and Medicine* **184**, 109310 (2025).
- [10] Zheng, L., Chen, H., Qing, L., Zhuang, J., Meng, B. and Xu, X., “Automatic Segmentation of Aortic and Mitral Valves for Heart Surgical Planning of Hypertrophic Obstructive Cardiomyopathy,” *Proceedings of the 15th Asian Conference on Machine Learning*, 1715–1730, PMLR (2024).
- [11] Huang, S.-C., Huo, Z., Steinberg, E., Chiang, C.-C., Lungren, M. P., Langlotz, C. P., Yeung, S., Shah, N. H. and Fries, J. A., “INSPECT: A Multimodal Dataset for Pulmonary Embolism Diagnosis and Prognosis,” [arXiv:2311.10798](https://arxiv.org/abs/2311.10798) (2023).
- [12] Isensee, F., Jaeger, P. F., Kohl, S. A. A., Petersen, J. and Maier-Hein, K. H., “nnU-Net: a self-configuring method for deep learning-based biomedical image segmentation,” *Nat Methods* **18**(2), 203–211 (2021).
- [13] Chen, J., Lu, Y., Yu, Q., Luo, X., Adeli, E., Wang, Y., Lu, L., Yuille, A. L. and Zhou, Y., “TransUNet: Transformers Make Strong Encoders for Medical Image Segmentation,” [arXiv:2102.04306](https://arxiv.org/abs/2102.04306) (2021).
- [14] Hatamizadeh, A., Nath, V., Tang, Y., Yang, D., Roth, H. R. and Xu, D., “Swin UNETR: Swin Transformers for Semantic Segmentation of Brain Tumors in MRI Images,” *Brainlesion: Glioma, Multiple Sclerosis, Stroke and Traumatic Brain Injuries*, A. Crimi and S. Bakas, Eds., 272–284, Springer International Publishing, Cham (2022).
- [15] Ma, J., He, Y., Li, F., Han, L., You, C. and Wang, B., “Segment anything in medical images,” *Nat Commun* **15**(1), 654 (2024).
- [16] Chen, J., Qian, L., Wang, P., Sun, C., Qin, T., Kalyanasundaram, A., Zafar, M., Elefteriades, J., Sun, W. and Liang, L., “A 3D Image Segmentation Study of U-Net on CT Images of the Human Aorta with Morphologically Diverse Anatomy,” [2024.10.02.616348](https://doi.org/10.4236/ojs.2024.10.616348) (2024).
- [17] Fedorov, A., Beichel, R., Kalpathy-Cramer, J., Finet, J., Fillion-Robin, J.-C., Pujol, S., Bauer, C., Jennings, D., Fennessy, F., Sonka, M., Buatti, J., Aylward, S., Miller, J. V., Pieper, S. and Kikinis, R., “3D Slicer as an image computing platform for the Quantitative Imaging Network,” *Magnetic Resonance Imaging* **30**(9), 1323–1341 (2012).
- [18] Liang, L., Liu, M., Elefteriades, J. and Sun, W., “PyTorch-FEA: Autograd-enabled finite element analysis methods with applications for biomechanical analysis of human aorta,” *Computer Methods and Programs in Biomedicine* **238**, 107616 (2023).
- [19] Liang, L., Liu, M., Martin, C., Elefteriades, J. A. and Sun, W., “A machine learning approach to investigate the relationship between shape features and numerically predicted risk of ascending aortic aneurysm,” *Biomech Model Mechanobiol* **16**(5), 1519–1533 (2017).